PHYSICS OF PLASMAS VOLUME 8, NUMBER 10 OCTOBER 2001
The following article appeared in Physics of Plasmas 8, number 10, pages 4608-4612, and may be found at http://link.aip.org/link/?php/8/4608

Nonstationary oscillations in gyrotrons

M. I. Airila* and O. Dumbrajs
Helsinki University of Technology, Euraton-Tekes Association, FIN-02015 HUT, Finland

A. Reinfelds and U. Strautiņš
Latvian Academy of Sciences and the University of Latvia, LV-1524 Riga, Latvia

(Received 25 April 2001; accepted 19 July 2001)

The onset of stochastic oscillations in gyrotrons is studied by means of the self-consistent theory describing nonstationary processes. Complicated alternating sequences of regions of stationary, automodulation, and chaotic oscillations are found in the plane of the generalized gyrotron variables: cyclotron resonance mismatch and dimensionless current. The results of the investigations are important in connection with attempts to increase the output power of gyrotrons by raising the current. © *2001 American Institute of Physics.* [DOI: 10.1063/1.1402173]

I. INTRODUCTION

In connection with striving to develop high-frequency high-power gyrotrons needed for modern fusion reactors it is appropriate to study under what circumstances chaos-like processes can occur in gyrotrons. Usually such operation regimes are undesirable for plasma physics applications. Here two types of stochasticity in gyrotrons should be distinguished: i) stochastic electron trajectories, ii) stochastic rf oscillations.

Stochastic electron trajectories have been studied in Refs. 1–3. In Ref. 1 it was found that in the case of a plane traveling wave of constant amplitude as force acting on electrons in a resonator no chaotic motions are possible. In Ref. 2 it was proved that in the cold-cavity approximation when the high-frequency field is represented by a Gaussian-type function, the solutions of the gyrotron equation are asymptotically equal to the solutions of the corresponding unforced equation. This means that chaos, which, in principle, can develop in a resonator for some values of control parameters, can be only transient, i.e., electrons again follow regular trajectories once they leave the interaction space. In Ref. 3 electron trajectories have been classified from the mathematical point of view and it has been shown that in real gyrotron resonators with a realistic strong aperiodic force the motion of the electrons in the vicinity of some particular initial angles is very sensitive with respect to the exact value of the initial angle. This sensitivity makes it possible to conclude that the trajectories of the electrons for these particular initial conditions may become chaotic, which means that there are electrons whose energy is virtually unpredictable after they leave the interaction space. The larger the current, the larger is the number of such electrons. It is clear that this adversely affects operation of depressed collectors and that such operation regimes should be avoided.

Stochastic rf oscillations have been studied in Refs. 4–6. In Ref. 4 equations have been derived which describe transition processes in rf generators operating near cut-off. Also the so-called reflectionless boundary condition has been formulated for the corresponding parabolic partial differential equation. In Refs. 5 and 6 this theory has been applied for gyrotrons and some sample calculations have been performed showing that in addition to stationary oscillations also periodic automodulation and stochastic oscillations are possible.

In the present work we reconsider the theory developed in Refs. 4–6. In particular, we use a much simpler method for solving the corresponding equations. By elaborate calculations we find complicated alternating sequences of regions of stationary, automodulation, and chaotic oscillations in the plane of the generalized gyrotron variables: cyclotron resonance mismatch and dimensionless current. The influence of the magnetic field tapering and the velocity spread of electrons on the topology of these regions is also examined.

II. GYROTRON EQUATIONS

To describe self-consistently the nonstationary oscillations one has to use the system of partial differential equations derived in Ref. 4:

$$\begin{cases} \dfrac{dp}{d\zeta} + i(\Delta + |p|^2 - 1)p = if(\zeta,\tau) \\ \dfrac{\partial^2 f}{\partial \zeta^2} - i\dfrac{\partial f}{\partial \tau} + \delta f = \dfrac{I}{2\pi}\displaystyle\int_0^{2\pi} p\,d\vartheta_0 \end{cases} \tag{1}$$

where p is the complex transverse momentum of the electron normalized to its initial absolute value, $\zeta = (\beta_{\perp 0}^2\omega/2\beta_{\|0}c)z$ is the dimensionless coordinate, $\beta_{\perp 0} = v_{\perp 0}/c$ and $\beta_{\|0} = v_{\|0}/c$ are normalized electron velocities, $\Delta = 2(\omega - \omega_c)/\beta_{\perp 0}^2\omega$ is the frequency mismatch, $\omega_c/2\pi = 28B/\gamma_{\rm rel}$ is the electron cyclotron frequency in GHz, B is the magnetic field in T, $\gamma_{\rm rel}$ is the relativistic factor of electrons, $f(\zeta)$ is the high-frequency field in the resonator, $\tau = \frac{1}{8}\beta_{\perp 0}^4\beta_{\|0}^{-2}\omega_c t$ is the dimensionless time, $\delta = 8\beta_{\|0}^2\beta_{\perp 0}^{-4}[\overline{\omega} - \omega(\zeta)]\omega_c^{-1}$ describes variation of the critical frequency $\omega(\zeta)$ along the resonator axis, $\overline{\omega}$ is the cut-off frequency at the exit from the resonator, and I is the dimensionless current,

$$I = 0.94 \times 10^{-4} I_0 \beta_{\|0}\beta_{\perp 0}^{-6} \frac{J_{m\pm 1}^2\left(\frac{2\pi}{\lambda}R_{el}\right)}{\gamma_{\rm rel}(\nu^2 - m^2)J_m^2(\nu)}. \tag{2}$$

* Electronic mail: markus.airila@hut.fi

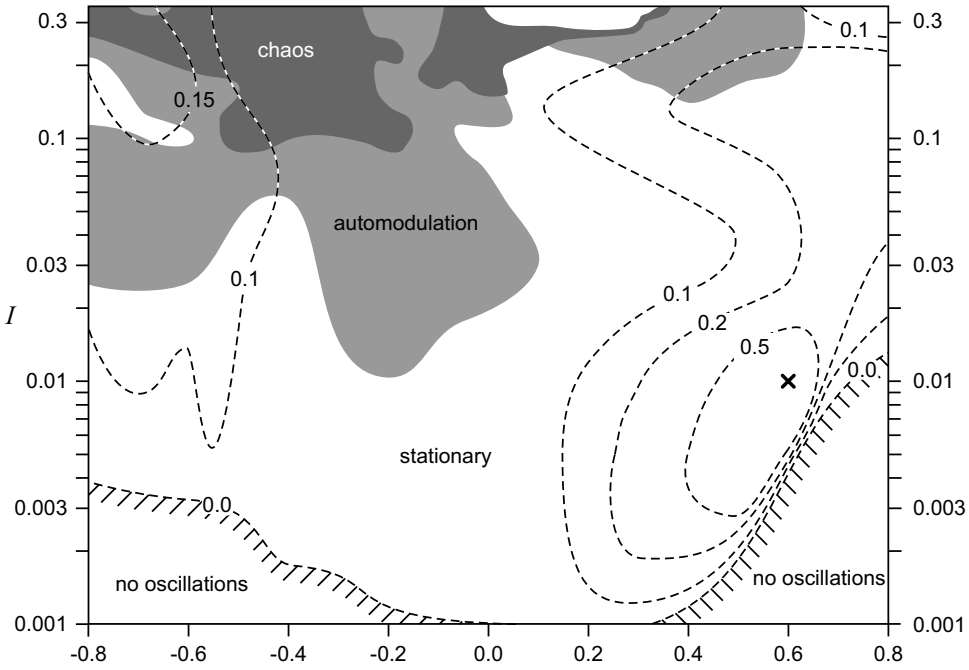

FIG. 1: Topology of different kinds of oscillations of a gyrotron in the $\Delta - I$ plane. White regions correspond to stationary oscillations, grey regions correspond to automodulation, and dark regions to chaotic oscillations. The contours of constant efficiency are shown by the dashed curves. The point of the maximum efficiency $\eta_\perp^{\max} = 0.75$ is marked by the cross.

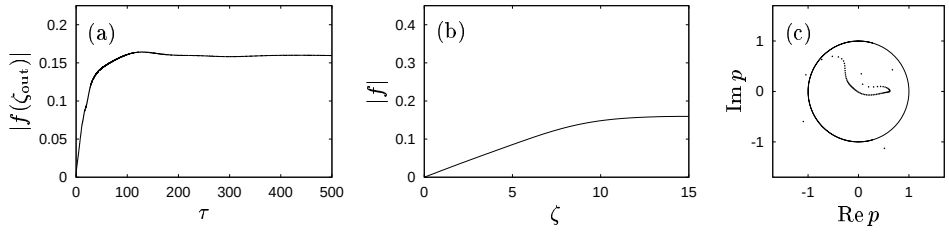

FIG. 2: $I = 0.01$, $\Delta = 0.60$. (a) Rf field amplitude at the resonator end as a function of time. (b) The stationary field profile in the cavity. (c) Phase space of 72 electrons after their passage through a resonator with a rf field profile shown in (b). The momentary and time-averaged perpendicular efficiencies coincide: $\eta_\perp = \langle \eta_\perp \rangle = 0.75$.

Here I_0 is current in Amperes, J is the Bessel function, m is the azimuthal index of the mode, λ is the wavelength, R_{el} is the electron beam radius, and ν is the zero of the derivative of the Bessel function. This description is valid for operation at the fundamental cyclotron resonance.

The system of equations (1) has to be supplemented by the standard initial condition for the momentum, $p(0) = \exp(i\vartheta_0)$ with $0 \le \vartheta_0 \le 2\pi$, and by the boundary condition for the field at the entrance to the interaction space:

$$f(0,\tau) = 0, \tag{3}$$

which means that at the entrance the field must vanish. At the exit from the interaction space ($\zeta = \zeta_{\rm out}$) the so-called reflectionless boundary condition is applied:

$$\left(f(\zeta,\tau) + \frac{1}{\sqrt{\pi i}} \int_0^\tau \frac{1}{\sqrt{\tau - \tau'}} \frac{\partial f(\zeta,\tau')}{\partial \zeta} d\tau' \right)\Big|_{\zeta=\zeta_{\rm out}} = 0. \tag{4}$$

The electron perpendicular efficiency $\eta_\perp$ which describes the extraction of the electron orbital momentum from the beam is given by the expression

$$\eta_\perp = 1 - \frac{1}{2\pi} \int_0^{2\pi} |p(\zeta_{\rm out})|^2 \, d\vartheta_0. \tag{5}$$

III. NUMERICAL METHOD

In Refs. 4–6 an unnecessarily complicated method based on Laplace transformations was used to solve the system of equations (1). We abandoned that method in favor of a much simpler and more transparent method based on the fully implicit scheme of solving parabolic differential equations:

$$\frac{f_{j+1}^{n+1} - 2f_j^{n+1} + f_{j-1}^{n+1}}{h^2} - i\frac{f_j^{n+1} - f_j^n}{\Delta\tau} + \delta f_j^{n+1} = g_j^n, \quad n = 0,1,\ldots;\ j = 1,\ldots,N-1, \tag{6}$$

where h is the spatial step, $\Delta\tau$ is the temporal step, $N = \zeta_{\rm out}/h$, $\tau_n = n\Delta\tau$, and

$$g_j^n = \sum_{k=1}^{s} \frac{Ip(\zeta_j, \tau_n, \vartheta_0^{(k)})}{s}. \tag{7}$$

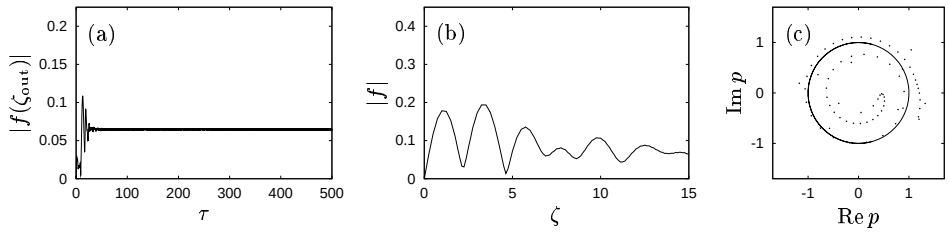

FIG. 3: $I = 0.15$, $\Delta = -0.80$, $\eta_\perp = \langle \eta_\perp \rangle = 0.15$. Other conventions same as in Fig. 2.

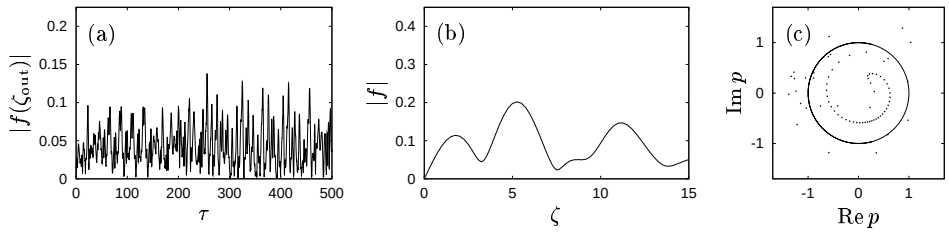

FIG. 4: $I = 0.15$, $\Delta = -0.30$, $\tau = 245$, $\eta_\perp = 0.30$, $\langle \eta_\perp \rangle = 0.04$. Other conventions same as in Fig. 2.

By noting that the singularity in the boundary condition (4) can be easily isolated if the function $\partial f(\zeta, \tau')/\partial\zeta$ satisfies the Lipschitz condition in the vicinity of τ, we can write a simple difference approximation of (4):

$$f_N^n + \frac{1}{\sqrt{\pi i}} \left(2\sqrt{\tau_n} \frac{f_N^n - f_{N-1}^n}{h} + \sum_{j=0}^{n-1} \frac{f_N^j - f_{N-1}^j - f_N^n + f_{N-1}^n}{h\sqrt{\tau_n - \tau_j}} \Delta\tau \right) = 0. \quad (8)$$

As a result we obtain a linear algebraic system of equations from which we can find $f_j^{n+1}, j = 1, 2, \ldots, N$ on the basis of the known values of f_j^n:

$$\begin{aligned} &\frac{1}{h^2} f_{j+1}^{n+1} - \left(\frac{2}{h^2} + \frac{i}{\Delta\tau} + \delta \right) f_j^{n+1} + \frac{1}{h^2} f_{j-1}^{n+1} \\ &= g_j^n - \frac{i}{\Delta\tau} f_j^n,\ j = 1, \ldots, N-1, \\ &\left(-2\sqrt{n+1} + \sum_{j=0}^{n} \frac{1}{\sqrt{n+1-j}} \right) f_{N-1}^{n+1} \\ &+ \left(\frac{h\sqrt{\pi i}}{\sqrt{\Delta\tau}} + 2\sqrt{n+1} - \sum_{j=0}^{n} \frac{1}{\sqrt{n+1-j}} \right) f_N^{n+1} \\ &= \sum_{j=0}^{n} \frac{f_{N-1}^j - f_N^j}{\sqrt{n+1-j}}. \end{aligned} \quad (9)$$

This system of equations is tridiagonal. It can be easily solved by the simple routine described in Ref. 7 by generalizing it to complex variables.

IV. COMPUTATIONS

The classification of the solutions of Eq. (1) is based on two criteria: temporal periodicity and variations of the amplitude of f. "Automodulation" refers to all periodic solutions, which we can detect by studying the autocorrelation function of the output. The autocorrelation function $R(t)$ of $A(\tau) = |f(\zeta_{\rm out}, \tau)|$ over the interval $(n_1\Delta\tau,\ n_2\Delta\tau)$ is defined as

$$R(n\Delta\tau) = \frac{1}{n_2 - n_1 - n} \times \sum_{k=n_1}^{n_2-n} \frac{[A(k\Delta\tau) - \langle A \rangle]\,[A(k\Delta\tau + n\Delta\tau) - \langle A \rangle]}{\langle A^2 \rangle - \langle A \rangle^2}, \quad (10)$$

where $n\Delta\tau$ is delay and $\langle A \rangle$ denotes the average of $A(\tau)$ computed over the interval $(n_1\Delta\tau,\ n_2\Delta\tau)$. Whenever $R(n\Delta\tau)$ shows a maximum $R(T) > 0.95$ [excluding R(0) = 1], the corresponding solution $A(\tau)$ is interpreted to be periodic with a period T.

Aperiodic solutions were further divided into chaotic ($T \to \infty$) and stationary ($T = 0$) ones. Based on a large number of numerical results, we concluded that the function $A(\tau)$ varies over a wide range of values whenever chaos appears. On the other hand, a stationary solution means that $A(\tau)$ stays constant. We can easily distinguish between these types of aperiodic solutions by imposing a numerical condition

$$\frac{\max A(\tau) - \min A(\tau)}{\max A(\tau)} < 0.1 \quad (11)$$

for stationary solutions, leaving the opposite for chaos. For both the autocorrelation function and the amplitude variations the time interval from $\tau_1 = 300$ to $\tau_2 = 500$ was used. This choice is a good compromise between avoiding initial transient oscillations in the data and performing the computations in a reasonable time. In some cases very slowly decaying oscillations confused the above-described automatic procedure and corrections by hand were needed.

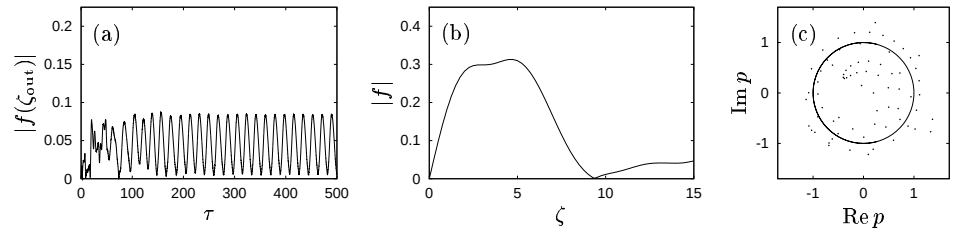

FIG. 5: $I = 0.15$, $\Delta = -0.05$, $\tau = 200$, $\eta_\perp = 0.07$, $\langle\eta_\perp\rangle = 0.06$. Other conventions same as in Fig. 2.

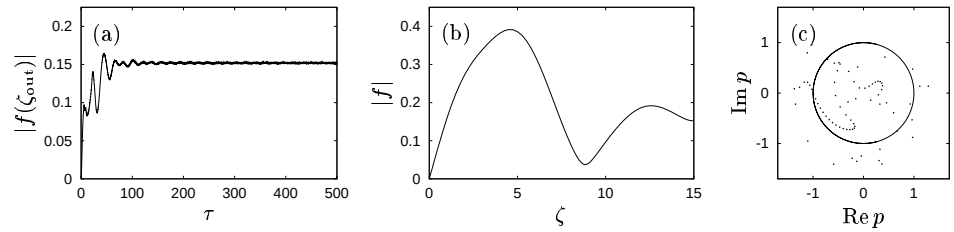

FIG. 6: $I = 0.15$, $\Delta = 0.30$, $\eta_\perp = \langle\eta_\perp\rangle = 0.19$. Other conventions same as in Fig. 2.

In the calculations we assumed that $\delta(\zeta) = 0$, $\zeta_{\rm out} = 15$, $h = 0.25$, $\Delta\tau = 0.02$, and used the following possible initial condition:

$$f(\zeta, 0) = 0.1 \sin\left(\pi \frac{\zeta}{\zeta_{\rm out}}\right) \tag{12}$$

which simulates the axial field profile with only one maximum.

V. RESULTS

In Fig. 1 we show the topology of different kinds of oscillations of a gyrotron in the $\Delta - I$ plane and the corresponding constant efficiency contours. Qualitatively we confirm the result obtained earlier in Refs. 5 and 6 that at low currents and in regions of high efficiency oscillations are stationary. [For the evolution of the output signal at the point of maximum efficiency, see Fig. 2(a).] However, the boundary between stationary and nonstationary oscillations (Fig. 6 of Ref. 5) gives no indication about the complicated topology beyond it. In particular, we find alternating sequences of stationary solutions, which is an fascinating mathematical property of the considered equations. For example, at $\Delta = -0.8$ or $\Delta = 0.05$ oscillations become again stationary at larger currents.

It is interesting to examine the axial structure of the field profile in the resonator and the phase space of the electron transverse momentum at the resonator exit. Figs. 2(b) and 2(c) illustrate these structures at the point of maximum efficiency ($I = 0.01, \Delta = 0.60$). The especially strong bunching of electrons which leads to high efficiency is clearly seen in Fig. 2(c). The case of resonance with the backward wave ($\Delta < 0$) is illustrated in Fig. 3; here $I = 0.15$ and $\Delta = -0.80$. The field profile has many maxima as a consequence of superposition of the backward wave with a forward wave resulting from a strong reflection at the input. In chaotic and automodulation regions illustrated in Fig. 4 ($I = 0.15, \Delta = -0.30$) and Fig. 5 ($I = 0.15, \Delta = -0.05$), respectively, the field profile varies very rapidly with time. To illustrate momentary field and phase space structures we have chosen arbitrary time values: $\tau = 245$ and $\tau = 200$, respectively. Of course, in the case of automodulation and stochasticity the momentary efficiencies deviate strongly from the time-averaged efficiencies. In Fig. 6 ($I = 0.15, \Delta = 0.30$) we show the case of stationary oscillations with very low efficiency. It is seen that in this case the field has two maxima [Fig. 6(b)] and that $|p| > 1$ for many electrons [Fig. 6(c)]. Finally in Fig. 7 ($I = 0.15, \Delta = 0.40$) we show automodulation with a small amplitude. The structures of the field profile and of the phase space are very similar to those shown in Fig. 6.

From Fig. 1 it is obvious that automodulation and chaotic oscillations occur at lower currents for negative values of Δ. For this reason it can be expected that a positive gradient of the magnetic field in the resonator would lower the current at which stochastic oscillations appear, because increasing magnetic field leads to decreasing effective Δ. Indeed, we can write

$$\Delta_{\rm taper} \approx \Delta \mp \frac{2}{\beta_\perp^2} \frac{\zeta}{\zeta_{\rm out}} \epsilon_B \tag{13}$$

where $\epsilon_B = (B_{\rm out} - B_0)/B_0$. Assuming a 5 % increase of the magnetic field inside the resonator ($\epsilon_B = 0.05$) and a typical value $\beta_\perp = 0.42$, we obtain

$$\Delta_{\rm taper} = \Delta - 0.567 \frac{\zeta}{\zeta_{\rm out}}. \tag{14}$$

Conversely, even a moderate magnetic field decrease would raise the threshold current for stochastic oscillations and thus improve the stability of gyrotron operation with respect to onset of stochastic oscillations.

The presented examples were also computed taking into account the velocity spread of electrons.[8] In general, the inclusion of spread changed the results very little. The solutions became qualitatively different only in the vicinity of boundaries of the regions shown in Fig. 1. This

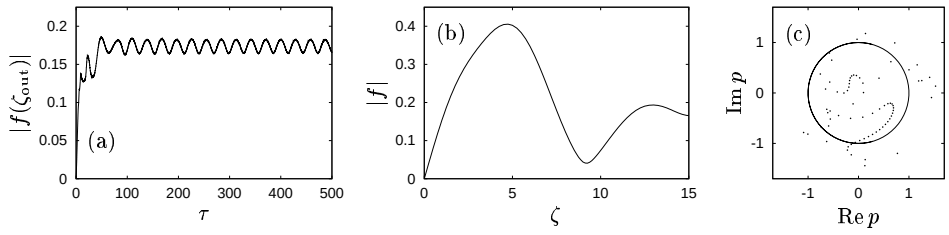

FIG. 7: $I = 0.15$, $\Delta = 0.40$, $\tau = 500$, $\eta_\perp = 0.22$, $\langle\eta_\perp\rangle = 0.23$. Other conventions same as in Fig. 2.

demonstrates that Fig. 1 can be used to roughly estimate the behavior of a gyrotron even in the presence of a 20 % velocity spread.

VI. FEASIBILITY OF EXPERIMENTAL CONFIRMATION OF THE RESULTS

Let us now estimate at what currents automodulation or chaos can be expected in realistic devices. As an example we consider the 2.2 MW, 165 GHz coaxial cavity gyrotron developed at Forschungszentrum Karlsruhe (Ref. 9). This gyrotron is operating in the $TE_{31,17}$ mode with a gun which delivers 84 A current and whose pitch factor at 90 kV is 1.3. Estimates based on Eq. (2) give $I = 0.003$, and the normalized interaction length $\mu = 17$ with a 18 mm cavity. On the one hand, this value of I shows that there is a large margin to raise the output power of a gyrotron by raising the current. On the other hand, it is clear that this gyrotron cannot be used to test the predictions shown in Figs. 3–7. For this purpose one would need to increase the current of the gun up to ~ 5000 A which, of course, is not realistic. As is evident from Eq. (2), the dimensionless current is inversely proportional to $\alpha\beta_\perp^5$, where $\alpha = \beta_{\perp 0}/\beta_{\|0}$. It is interesting to note that during the startup of this gyrotron the working mode $TE_{31,17}$ passes through the automodulation region ($\Delta = -0.25$ and $I = 0.042$ at 60 kV; $\Delta = 0.01$ and $I = 0.027$ at 65 kV) before reaching the operating point $\Delta = 0.47$ and $I = 0.003$ at 90 kV. The calculations performed in Ref. 9 show that due to mode competition these automodulation oscillations probably cannot be observed, since it is expected that they will be suppressed by competing modes which have much more favorable values of Δ and I. Such oscillations could be observed in special experiments in which the magnetic compression and thus the electron orbital velocity in the cavity would be decreased leading to large increase of I.

It should be easier to check the predictions shown in Fig. 1 in gyrotrons operating in low-order modes, because for such modes the dimensionless current is much larger for comparable values of the current of the gun. Moreover, mode selection becomes simpler due to a rarer spectrum.

In some special applications (material processing, special-purpose radars) chaotic oscillations are desirable. From Fig. 1 it is obvious that under normal circumstances (reasonable currents, high efficiency, high power) stochastic oscillations cannot be generated. However, it is known (Ref. 10) that artificially introduced reflections significantly decrease currents at which stochasticity begins to manifest itself. Within the framework of the theory considered in this paper such reflections can be modeled by means of the function $\delta(\zeta)$.

VII. CONCLUSIONS

The onset of stochastic oscillations in gyrotrons has been reconsidered. A simple and straightforward numerical method for solving the system of underlying partial differential equations has been used. It has been found that the topology of the domains of different kinds of oscillations is more complicated than envisaged earlier. In particular, alternating sequences of regions of stationary, automodulation and chaotic regions are found in the plane of the generalized gyrotron variables: frequency mismatch and dimensionless current. There is a large margin for increasing output power by raising the current without a risk of induction of stochastic oscillations.

ACKNOWLEDGMENT

We wish to thank G. S. Nusinovich for discussions and useful suggestions.

[1] P. A. Lindsay and X. Chen, IEEE Trans. Plasma Sci. **22**, 834 (1994).
[2] O. Dumbrajs, R. Meyer-Spasche, and A. Reinfelds, IEEE Trans. Plasma Sci. **26**, 846 (1998).
[3] M. I. Airila, O. Dumbrajs, A. Reinfelds, and D. Teychenné, Int. J. Infrared Millim. Waves **21**, 1759 (2000).
[4] N. S. Ginzburg, N. A. Zavolsky, G. S. Nusinovich, and A. S. Sergeev, Izv. Vyssh. Uchebn. Zaved., Radiofiz. **29**, 106 (1986) [Sov. Radiophys., Quantum Electron. **29**, 89 (1986)].
[5] N. S. Ginzburg, G. S. Nusinovich, and N. A. Zavolsky, Int. J. Electron. **61**, 881 (1986).
[6] N. S. Ginzburg, N. A. Zavolsky, and G. S. Nusinovich, Radiotekh. Elektron. (Moscow) **32**, 1031 (1987) [Sov. J. Commuun. Technol. Electron. **32**, 132 (1987)].
[7] W. H. Press, S. A. Teukolsky, W. T. Vetterling, and B. P. Flannery, *Numerical Recipes in FORTRAN. The Art of Scientific Computing* (Cambridge University Press, New York, 1994), p. 43.
[8] M. I. Airila and O. Dumbrajs, Phys. Plasmas **8**, 1358 (2001).
[9] B. Piosczyk, A. Arnold, G. Dammertz, O. Dumbrajs, M. Kuntze, W. Leonhardt, A. B. Pavelyev, M. Schmid, and M. Thumm, in *Conference Digest, 25th International Conference on Infrared and Millimeter Waves, Beijing, 2000*, edited by S. Liu and X. Shen (IEEE Press, Beijing, 2000), p. 19.
[10] N. S. Ginzburg, M. Yu. Glyavin, M. A. Moiseev, Yu. V. Novozhilova, N. A. Zavolsky, and V. E. Zapevalov, Pis'ma Zh. Tekh. **24**, 53 (1998) [Tech. Phys. Lett. **24**, 436 (1998)].